



Pergamon

J. Mech. Phys. Solids, Vol. 46, No. 10, pp. 2049–2068, 1998

© 1998 Elsevier Science Ltd. All rights reserved

Printed in Great Britain

0022-5096/98 \$—see front matter

PII: S0022-5096(98)00018-0

THE MECHANICS OF SIZE-DEPENDENT INDENTATION

MATTHEW R. BEGLEY^a and JOHN W. HUTCHINSON^{*,b}

^a Department of Mechanical Engineering, University of Connecticut, Storrs, CT 06269-3139, U.S.A.

^b Division of Engineering and Applied Sciences, Harvard University, Cambridge, MA 02138, U.S.A.

(Received 20 December 1997; in revised form 23 January 1998)

ABSTRACT

Indentation tests at scales on the order of one micron have shown that measured hardness increases significantly with decreasing indent size, a trend at odds with the size-independence implied by conventional plasticity theory. In this paper, strain gradient plasticity theory is used to model materials undergoing small-scale indentations. Finite element implementation of the theory as it pertains to indentation modeling is briefly reviewed. Results are presented for frictionless conical indentations. A strong effect of including strain gradients in the constitutive description is found with hardness increasing by a factor of two or more over the relevant range of behavior. The results are used to investigate the role of the two primary constitutive length parameters in the strain gradient theory. The study indicates that indentation may be the most effective test for measuring one of the length parameters. © 1998 Elsevier Science Ltd. All rights reserved.

Keywords: A. indentation and hardness, B. elastic–plastic material, C. finite elements.

1. INTRODUCTION

Indentation tests have been used extensively to characterize the plastic properties of solids. Historically, one of the primary goals of indentation testing has been to estimate the yield stress by measuring the hardness, defined as the load on the indenter divided by the area of the resulting impression (e.g. Atkins and Tabor, 1965; Johnson, 1970; Rubenstein, 1981). Recently, hardness has been shown to be size-dependent when the width of the impression is below about fifty microns. Such small-scale experiments are often referred to as micro-indentation tests (or nano-indentation tests at the sub-micron scale) and have become a popular method of illustrating the size-dependence of plastic deformation (Gane and Cox, 1970; Pethica *et al.*, 1983; Doerner and Nix, 1986; Samuels, 1986; Stelmashenko *et al.*, 1993; Atkinson, 1995; Ma and Clark, 1995; Poole *et al.*, 1997). The measured hardness may double or even triple as the size of indent decreases from about fifty microns to one micron. In effect, the smaller the scale the stronger the solid. This is a large effect which almost certainly has significant implications for other applications of metal plasticity at the micron scale. A size-dependence of indentation hardness is not encompassed by conventional plasticity. Simple arguments, based on dimensional analysis, reveal that any plasticity

* To whom correspondence should be addressed. E-mail: hutchinson@husm.harvard.edu

theory which does not contain a constitutive length parameter will predict size-independent indentation hardness.

Recently, new plasticity theories containing constitutive length scales have been developed to characterize size-dependent plastic deformation (e.g. Fleck and Hutchinson, 1993, 1996; Acharya and Bassini, 1996, 1997). Micro-hardness tests are thought to provide an effective method for characterizing a material's flow response at small length scales. By correlating an indentation solution for a given theory with test data in the size-dependent range, one should be able to infer values of the constitutive length parameters, in much the same way as the macroscopic hardness test is used to measure flow stress.

In this paper, the Fleck–Hutchinson (1997) strain gradient plasticity theory has been used to determine the effect of the material length scale on predicted hardness for small indents. Prior to this work, only one attempt appears to have been made to analyze the size-dependence of micro-hardness tests with a continuum theory of strain gradient plasticity. Shu and Fleck (1996) applied an earlier version of the plasticity theory that accounts for contributions of rotation gradients to hardening but not of stretch gradients. They found that a version of the theory based on rotation gradients alone cannot account for the strong size-dependence observed experimentally. In part, their finding provides the motivation for the present work which extends the study to include the role of stretch gradients. In addition, contact will be made between the present results and predictions from dislocation-based models of micro-indentation size-dependence by Ma and Clarke (1995), Brown (1997) and Nix (1997).

The constitutive behavior and its finite element implementation are first briefly reviewed. Results are then presented for conical indentation without friction. The two primary goals of this paper are: (a) to assess the effectiveness of strain gradient plasticity theory in accounting for the strong size-dependence observed in indentation tests; and (b) to infer values of the constitutive length parameters via correlation of the mechanics results with experimental data available in the literature.

2. CONSTITUTIVE DESCRIPTION

The constitutive behavior of the material is described within the context of small strains and small rotations. A deformation theory version of strain gradient plasticity is used here in the form given by Fleck and Hutchinson (1997). The formulation is for a small strain, non-linear elastic solid, where both strain and strain gradients contribute to the strain energy density. It falls within the general class of solids considered by Toupin (1962) and Mindlin (1965). Interpretation of the strain gradient contribution to strain hardening in terms of the connection of strain gradients to the generation of geometrically necessary dislocations has been discussed by Fleck *et al.* (1994).

The strain tensor is defined in terms of the displacements u_i in the usual manner, that is $\varepsilon_{ij} = \frac{1}{2}(u_{i,j} + u_{j,i})$. The second gradient of the displacement vector is defined as $\eta_{ijk} = u_{k,ij}$; it can be expressed in terms of the strain gradients as $\eta_{ijk} = \varepsilon_{jk,i} + \varepsilon_{ik,j} - \varepsilon_{ij,k}$. The effective strain measure introduced below is taken to be a function of only the deviatoric parts of the strain and strain gradient tensors, defined as

$$\varepsilon'_{ij} = \varepsilon_{ij} - \frac{1}{3} \delta_{ij} \varepsilon_{kk} \quad (1a)$$

$$\eta'_{ijk} = \eta_{ijk} - \frac{1}{4} (\delta_{ik} \eta_{jpp} + \delta_{jk} \eta_{ipp}) \quad (1b)$$

such that $\eta'_{ikk} = 0$. Non-zero deviatoric strain gradients for the general axisymmetric case are given in terms of the displacements in the Appendix. Smyshlaev and Fleck (1995) showed that the deviatoric strain gradient tensor could be decomposed into three unique, mutually orthogonal third order deviatoric tensors according to $\eta'_{ijk} = \eta_{ijk}^{(1)} + \eta_{ijk}^{(2)} + \eta_{ijk}^{(3)}$, where $\eta_{ijk}^{(m)} \eta_{ijk}^{(n)} = 0$ for $m \neq n$ and each tensor preserves the properties $\eta_{ijk}^{(m)} = \eta_{jik}^{(m)}$ and $\eta_{ikk}^{(m)} = 0$. The steps required to carry out this decomposition are also given in the article by Fleck and Hutchinson (1997).

The effective strain measure used to define the deformation theory is taken to be the isotropic invariant

$$E_e^2 = \frac{2}{3} \varepsilon'_{ij} \varepsilon'_{ij} + l_1^2 \eta_{ijk}^{(1)} \eta_{ijk}^{(1)} + l_2^2 \eta_{ijk}^{(2)} \eta_{ijk}^{(2)} + l_3^2 \eta_{ijk}^{(3)} \eta_{ijk}^{(3)}. \quad (2)$$

The first term in (2), $\frac{2}{3} \varepsilon'_{ij} \varepsilon'_{ij}$, is the invariant used to form the classical J_2 deformation theory, and the strain gradient theory reduces to the classical theory in the limit in which the strain gradients are small. The three invariants of the strain gradients in (2) represent the most general dependence on the deviatoric strain gradient tensor that is isotropic and homogeneous of degree two. The contribution is positive definite when the three length quantities, l , are each non-zero. These lengths are the new constitutive parameters in the theory.

It is instructive to write the effective strain in a form which reveals more explicitly its dependence on rotation gradients. With the rotation as $\theta_i = \frac{1}{2} e_{ijk} u_{k,j}$, where e_{ijk} is the permutation tensor, define $\chi_{ij} = \theta_{i,j} = e_{ipk} \varepsilon'_{kjp}$ as the rotation gradient. As Fleck and Hutchinson (1997) have noted, the second and third of the above strain gradient invariants depend only on the rotation gradients:

$$\eta_{ijk}^{(2)} \eta_{ijk}^{(2)} = \frac{4}{3} \chi_{ij} \chi_{ij} + \frac{4}{3} \chi_{ij} \chi_{ji} \quad \text{and} \quad \eta_{ijk}^{(3)} \eta_{ijk}^{(3)} = \frac{8}{5} \chi_{ij} \chi_{ij} - \frac{8}{5} \chi_{ij} \chi_{ji} \quad (3)$$

Thus, an equivalent alternative expression to (2) is

$$E_e^2 = \frac{2}{3} \varepsilon'_{ij} \varepsilon'_{ij} + l_1^2 \eta_{ijk}^{(1)} \eta_{ijk}^{(1)} + \frac{2}{3} l_{CS}^2 \chi_{ij} \chi_{ij} + \left(\frac{4}{3} l_2^2 - \frac{8}{5} l_3^2 \right) \chi_{ij} \chi_{ji} \quad (4)$$

where $l_{CS}^2 = (2l_2^2 + 12l_3^2/5)$. The invariant $\eta_{ijk}^{(1)} \eta_{ijk}^{(1)}$ depends on both stretch and rotation gradients. For deformations which are irrotational (i.e. $\chi_{ij} = 0$), only the first of the length parameters, l_1 , has any influence. It is through $l_1^2 \eta_{ijk}^{(1)} \eta_{ijk}^{(1)}$ that stretch gradients make their presence felt.

The first version of the strain gradient theory (Fleck *et al.*, 1994; Fleck and Hutchinson, 1994) assumed strain gradients enter only through the one invariant of the rotation gradients, $\chi_{ij} \chi_{ij}$, according to

$$E_e^2 = \frac{2}{3} \varepsilon'_{ij} \varepsilon'_{ij} + \frac{2}{3} l_{CS}^2 \chi_{ij} \chi_{ij}. \quad (5)$$

This is a special case of (4) with $l_1 = 0$, $l_2 = \frac{1}{2} l_{CS}$ and $l_3 = \sqrt{\frac{5}{24}} l_{CS}$. This class of solids falls within the framework of couple stress theory, a sub-set of Toupin–Mindlin theory. Fleck *et al.* (1994) analyzed wire torsion data for annealed copper wires ranging in radius from 7–60 microns using the version of the plasticity theory based

on (5). By fitting the theory to the data, they inferred that $l_{CS} \cong 4 \mu\text{m}$ for this material. The deformations in wire torsion are such that the two other invariants of the strain gradients in (4), $\eta_{ijk}^{(1)}\eta_{ijk}^{(1)}$ and $\chi_{ij}\chi_{ji}$, are identically zero (Fleck and Hutchinson, 1997). Thus, for this application, there is no loss in generality in using a theory based on (5) rather than (4). In other applications, however, contributions from stretch gradients through $l_1^2\eta_{ijk}^{(1)}\eta_{ijk}^{(1)}$ can be of dominant importance, particularly when deformations are nearly irrotational. Examples of this type discussed by Fleck and Hutchinson (1997) include void growth and cavitation, crack tip fields, and indentation.

No examples have been identified yet for which the third invariant of the strain gradients in (4), $\chi_{ij}\chi_{ji}$, plays a particularly important role. To reduce the set of length parameters from three to two, we will exclude any dependence on $\chi_{ij}\chi_{ji}$ in (4) by taking $l_2 = \sqrt{6/5}l_3$ (with $l_2 = l_{CS}/2$ and $l_3 = \sqrt{5/24}l_{CS}$) such that (4) becomes

$$E_e^2 = \frac{2}{3}e'_{ij}e'_{ij} + l_1^2\eta_{ijk}^{(1)}\eta_{ijk}^{(1)} + \frac{2}{3}l_{CS}^2\chi_{ij}\chi_{ij}. \quad (6)$$

From (2), it can be noted that this combination is positive definite if both l_1 and l_{CS} are non-zero. As mentioned above, l_{CS} controls the size effect in wire torsion, while the outcome of the present work will be that l_1 is by far the more important of the two parameters in micro-indentation. Thus, it seems likely that both length parameters, l_1 and l_{CS} , must be retained for general application of the theory. Moreover, unless it turns out that these two length parameters have fixed proportion for all metals, it would appear that experimental data from at least two different types of small scale tests will be required to separately determine l_1 and l_{CS} . Further discussion of this issue will be given at the end of the paper.

A strain energy density function is assumed in the form

$$W(E_e) = w(E_e) + \frac{E}{6(1-2\nu)}e_{ii}^2 \quad (7)$$

where E is Young's modulus and ν is Poisson's ratio. The dependence on deviatoric quantities $w(E_e)$ is chosen such that in uniaxial tension the stress-strain behavior derived from (7) reproduces the Ramberg-Osgood tensile relation

$$\varepsilon = \frac{\sigma}{E} + \frac{3}{7} \frac{\sigma_y}{E} \left(\frac{\sigma}{\sigma_y} \right)^n. \quad (8)$$

The work increment per unit volume associated with an arbitrary variation of the displacements is

$$\delta W = \sigma_{ij}\delta\varepsilon_{ij} + \tau_{ijk}\delta\eta_{ijk} \quad (9)$$

where the stress quantities, $\sigma_{ij} = \sigma_{ji}$ and $\tau_{ijk} = \tau_{jik}$, are obtained from W by

$$\sigma_{ij} = \frac{\partial W}{\partial \varepsilon_{ij}} \quad \text{and} \quad \tau_{ijk} = \frac{\partial W}{\partial \eta_{ijk}}. \quad (10)$$

The principle of virtual work is given by

$$\int_V [\sigma_{ij}\delta\varepsilon_{ij} + \tau_{ijk}\delta\eta_{ijk}] dV = \int_V f_i\delta u_i dV + \int_S [t_i\delta u_i + r_i n_j\delta u_{i,j}] dS \quad (11)$$

where dV and dS are the volume and surface elements, f_i is the body force per unit volume, t_i is the surface traction, r_i is the double stress traction, and n_i is unit surface normal. The equilibrium relationship derived from the principle is

$$\sigma_{ik,i} - \tau_{ijk,ij} = -f_k \quad (12a)$$

while the stress–traction relationships for a straight boundary aligned with the x_1 axis are

$$t_k = \sigma_{2k} - \tau_{2jk,j} - \tau_{21k,1} \quad (12b)$$

$$r_k = \tau_{22k}. \quad (12c)$$

Stress–traction relationships for arbitrarily oriented and shaped boundaries are given by Fleck and Hutchinson (1997).

3. FINITE ELEMENT FORMULATION AND INDENTATION MODEL

On the basis of the deformation strain gradient plasticity behavior outlined in the previous section, a finite element scheme was derived for the general axisymmetric case. The potential energy of the system is given by

$$\pi(u) = \int_V \left[w(E_e) + \frac{1}{2} \kappa \left(\frac{\varepsilon_{ii}}{3} \right)^2 \right] dV - \int_S [t_k u_k + r_k D u_k] dS \quad (13)$$

where $\kappa = E/(3(1-2\nu))$ is the bulk modulus and S is the portion of the boundary on which tractions are prescribed. The principle of minimum potential energy applies in the usual manner, i.e. of all kinematically admissible displacement fields, the actual displacement field will render π a minimum. The governing equations are then found by taking the first variation of (14) in the usual manner. The finite element discretization of the result follows standard procedures, but is complicated by the dependence of w on strain gradients.

The finite element model is illustrated in Fig. 1. The contact radius is defined as a ; the depth of penetration of the indenter is δ . The half-angle of the indenter, β , was taken to be 72° , which corresponds to a Vickers indenter. The indenter is assumed to be rigid. Contact between the indenter and the substrate is assumed to be frictionless. Studies on conventional elastic–plastic solids indicate little difference between the hardness predicted for a frictionless indenter and that for an indenter–substrate system permitting no sliding. The material is modeled as being a semi-infinite half plane; the size of the mesh was chosen by decreasing the size relative to the contact radius until there was a negligible change in the calculated hardness.

3.1. Choice of element

It is important to note that admissibility requirements of the second gradient terms require C_1 continuity in displacements. Previous strain gradient modeling efforts have explored a variety of types of elements (Xia and Hutchinson, 1996) and have shown that element performance is strongly dependent on the constitutive behavior. Based

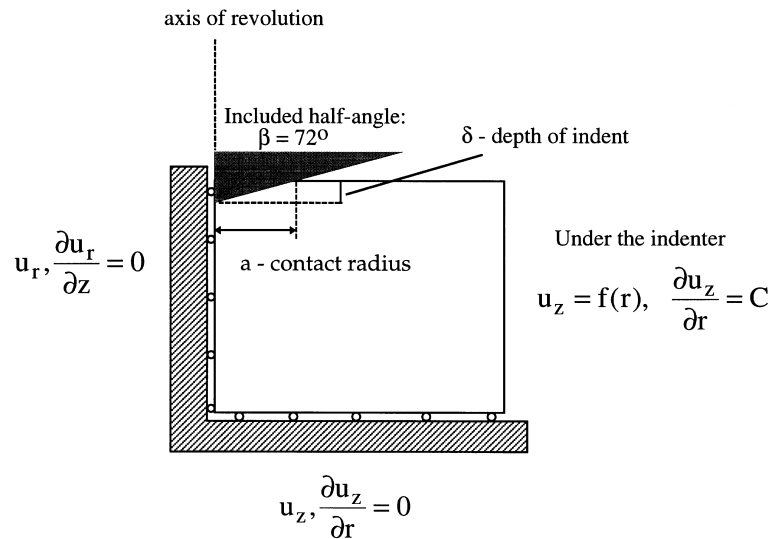


Fig. 1. Geometry of the axisymmetric indentation model and boundary conditions.

on this earlier work, an element similar to one initially derived for plate applications was chosen; problems in previous work (Xia and Hutchinson, 1996) with the element concerning adequate hydrostatic stress fields did not arise for the compressible material modeled here. More recently, C_0 elements with displacement gradients as nodal degrees of freedom have been investigated and performed admirably for linear elastic boundary value problems; these elements may prove more desirable for future efforts in strain gradient plasticity (Shu *et al.*, 1997).

The element is a three noded triangle with eighteen degrees of freedom. For each node, the nodal variables are

$$u_r, \frac{\partial u_r}{\partial r}, \frac{\partial u_r}{\partial z}, u_z, \frac{\partial u_z}{\partial r}, \frac{\partial u_z}{\partial z}. \quad (14)$$

Thus, the elements produce C_1 continuity at the nodes. The shape functions were derived by Specht (1988) and are outlined and discussed by Zienkiewicz and Taylor (1989). In general, the displacement gradients are not continuous across element boundaries, only at the nodes. However, the variation of displacement gradients along element faces are defined such that the element passes the patch test and can exactly reproduce constant strain gradient fields. This implies that there is no spurious energy contribution from jumps in displacement gradients across element boundaries.

The constitutive behavior and interpolation outline above were used in defining a general axisymmetric user element in the commercial code ABAQUS.

3.2. Boundary conditions

Axisymmetry dictates that u_r and $\partial u_r / \partial z$ are zero along the axis of symmetry. The vertical displacement along the bottom of the mesh was constrained to be zero,

while the radial quantities were unconstrained. Derivatives of displacements must be specified in addition to displacements, as they are additional nodal degrees of freedom.

For a frictionless indenter, the proper boundary condition underneath the indenter is a constraint between the radial and vertical displacements; the nodes in the contact region are constrained to fall on the indenter, with freedom to slide up and down the face of the indenter. For small strain theory and the shallow indenters considered here, this can be approximated by specifying the downward displacement and allowing the radial displacement to be free. The more shallow the indenter, the more accurate are these linearized boundary conditions. Thus, the following modified boundary conditions under the indenter were imposed:

$$(i) \quad u_z(r) = -\delta + \frac{r}{\tan \beta}, \quad \frac{\partial u_z}{\partial r} = \frac{1}{\tan \beta} \quad (15a)$$

$$(ii) \quad \text{no restriction on } u_r, \quad \frac{\partial u_r}{\partial r}, \quad \frac{\partial u_r}{\partial z}, \quad \frac{\partial u_z}{\partial z}. \quad (15b)$$

In addition to approximating zero shear traction under the indenter, (15b) results in a zero double stress traction [given by (12c)], enforced by the variational principle.

3.3. Determining the proper contact radius and indent depth

The contact between the indenter and the substrate was simulated by assuming a contact radius, a , and iterating to find the proper indentation depth, δ , for that size of indent. The proper indentation depth is defined as the depth at which the normal pressure between the indenter and material goes to zero at the edge of contact, i.e. at $r = a$. Using small strain theory for shallow indenters, the pressure is given by the traction in the vertical direction, given by (12b). The pressure under the indenter simplifies to

$$t_z = \sigma_{zz} - 2 \frac{\partial \tau_{rz}}{\partial r} - \frac{\partial \tau_{zz}}{\partial z}. \quad (16)$$

For the strain gradient solid, evaluating the tractions under the indenter using (16) and the finite element solution proved unreliable, due to the difficulty in evaluating the derivatives of the higher order stress quantities. To avoid this, the correct depth was assumed to be that at which the nodal forces went to zero at the edge of contact. Since the nodal forces represent the integrated average of the tractions over the element faces, this is consistent with the zero-traction criterion. The benchmark test results summarized below confirm the accuracy of this method.

3.4. Benchmark tests

The element performance and mesh geometry were tested by comparing predicted hardness values with an analytical solution for shallow conical indentation of an elastic half-space and some results based on conventional plasticity for the same problems which were presented by Shu and Fleck (1996). In general, the model was quite accurate. There was less than 2% error in the indentation load at a given indentation radius compared with the analytical solution for the elastic problem. The

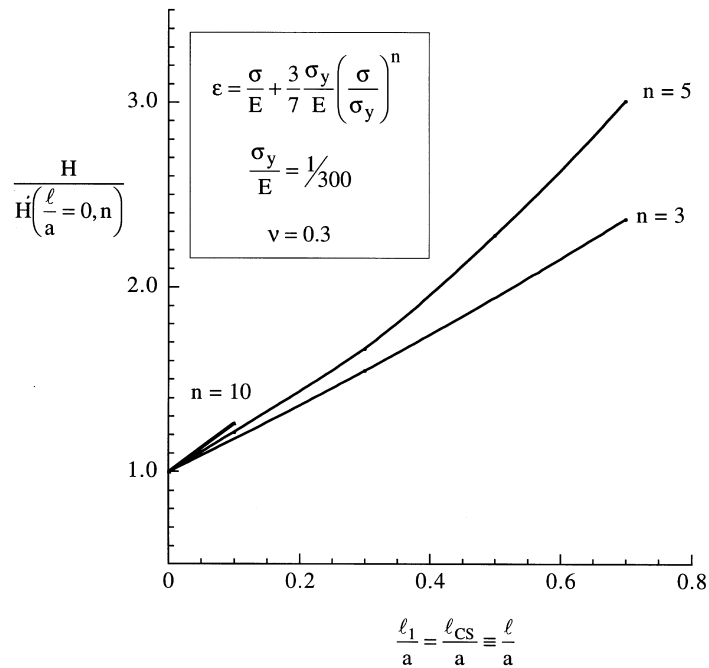


Fig. 2. Size-dependent hardness predictions as a function of material length scale over contact radius, for a frictionless conical indenter with a 72° half-angle.

hardness values (loads) for conventional plasticity were within 5% of the benchmark tests outlined by Shu and Fleck (1997).

The added computational expense of six degrees of freedom per node was partially compensated by the greater accuracy of the higher order element. The mesh density was chosen by examining the hardness values as the size of the smallest element (located adjacent to the contact radius) decreased. For both the conventional and strain gradient theories, the change in hardness was less than several percent when the minimum element size was decreased from $0.034a$ to $0.016a$; decreasing the minimum element size further by a factor of two led to even smaller changes in predicted hardness, although computation time increased significantly. The mesh used to generate the results was comprised of 1500 elements, with a minimum element size of $0.016a$.

4. NUMERICAL RESULTS

4.1. Size-dependent hardness

Computed size-dependent hardness for the conical indenter with a half-angle $\beta = 72^\circ$ is presented in Fig. 2, where the hardness H is defined as $P/(\pi a^2)$ with P as the load. These results are for the strain gradient solid with $l_1 = l_{CS} \equiv l$ for several

Table 1. Values of the material length scale determined from least squares fits with several experiments from the literature

	Orientation	Macroscopic hardness— H_0 MPa	$n = 3$ μm	$n = 5$ μm
Stelmashenko <i>et al.</i> (1993)	(100)[011]	3100	0.52	0.41
	(110)	3200	0.38	0.32
	(111)[011]	3300	0.25	0.22
Ma and Clarke (1995)	[100]	360	0.39	0.34
	[110]	375	0.22	0.19
Nix (1997)		566	0.60	0.42
Atkinson (1995)	Work-hardened		0.81	0.73
	Annealed		1.76	1.56

values of the hardening exponent n . The particular solid with $l_1 = l_{CS} \equiv l$ hardens in response to both stretch and rotation gradients. It was labeled an SG solid by Fleck and Hutchinson (1997) and was used in that paper to study the effect of strain gradients in several examples. Emphasis is on the variation of hardness with relative size of the indent as measured by the ratio of the indent radius to the material length parameter l . The results in this paper have been computed with $\sigma_y/E = 1/300$ and $\nu = 0.3$.

The hardness, H , in Fig. 2 has been normalized by the conventional plasticity result at the same value of n , i.e. the limiting result for $l/a \rightarrow 0$, which is given in Table 2 in the Appendix. The values for the conventional limit in Table 2 can be used with Fig. 2 to determine the actual hardness for a given length scale or size of indent. The plot thus represents the relative increase in hardness due to including strain gradients in the constitutive formulation. The abscissa in Fig. 2 is l/a , and it can be seen that size-dependent increases in hardness begin to become significant when a is less than about $10l$. Hardness is approximately doubled for indentation radii as small as about twice the length scale parameter l . The relative increase in hardness for $n = 5$ is greater than for $n = 3$, although the absolute increase in hardness at corresponding values of l/a are very nearly the same for the two strain hardening levels. In Section 5, the absolute value of the material length parameter will be estimated by comparison with experiments available in the literature.

4.2. Deformation characteristics

The deformed surface profiles under the indenter are shown in Fig. 3(a) for several indent sizes. In this figure, the radial and vertical locations have been normalized by the material length scale, which is assumed to be a material property. The values of the indent load (labeled in the figure) and displaced profiles accent the role of the normalizations used in calculating the hardness. The hardness, which is defined as the average stress under the indenter, is a function of the size of indent relative to the material property l , as already noted.

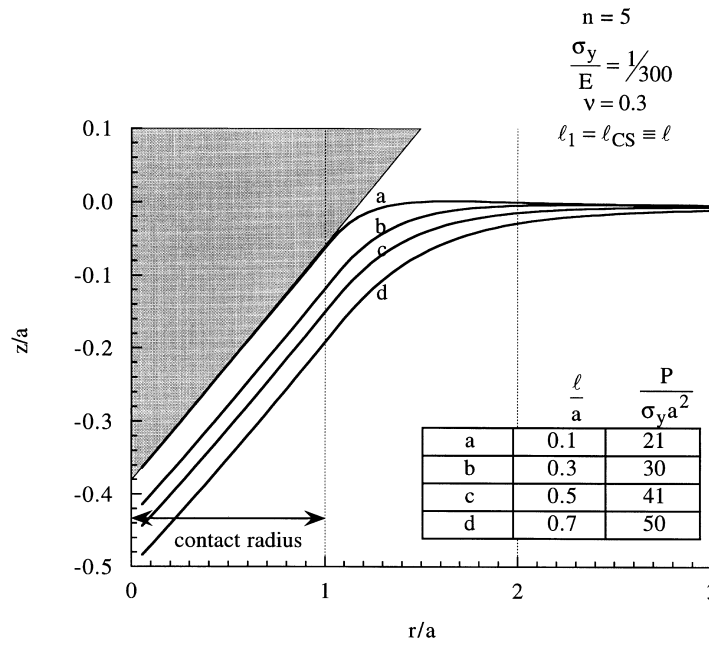
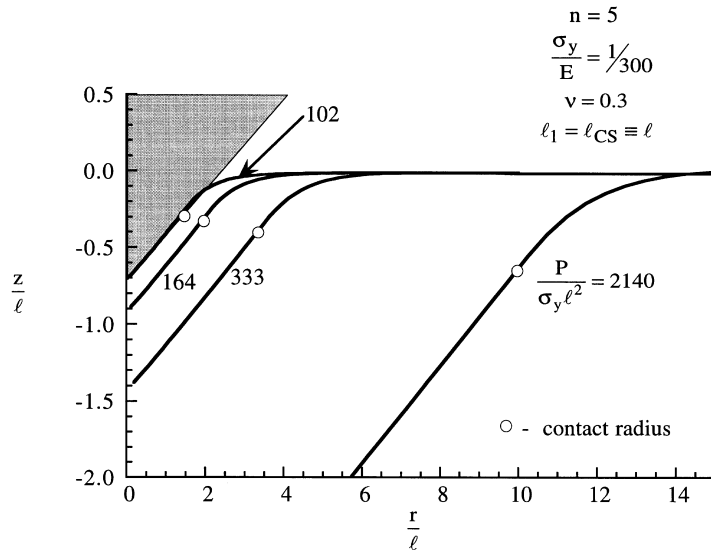


Fig. 3. (a) Deformed surface profiles for several indent sizes and constant material length scale. Given in the figure are normalized values of the indent load. (b) Deformed surface profiles for constant indent size and various length scales. Given in the figure are normalized values of material length scale and corresponding indent load.

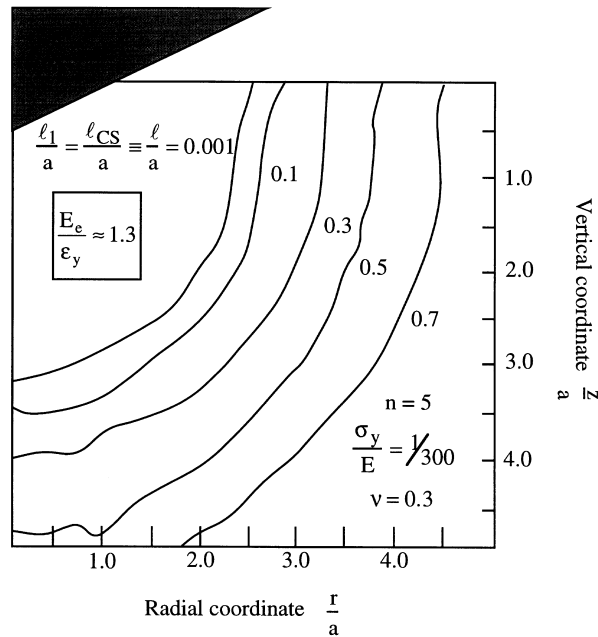


Fig. 4. Effective strain contours for various material length scales; each curve represents the estimated plastic zone size (i.e. $E_e \approx 1.3\epsilon_y$) for a given length scale to indent size ratio.

Figure 3(b) illustrates the effect of variations of material length parameter at constant indent size. These cases can be considered to be indents of the same size (defined as having the same contact radius) in materials with different length parameters l . The materials with the larger l are harder, and require greater loads to create the same contact radius. This is consistent with both the experimental behavior and anticipated behavior of the constitutive description, which dictates that the amount of hardening increases as l increases. The curves show that this increased hardening results in profiles that are increasingly similar to the elastic case where no pile-up occurs.

The effect of the material length parameter on the amount of plasticity underneath the indenter can be investigated by estimating the size of the plastic zone under the indenter. In Fig. 4, approximate boundaries to the plastic zone are shown for several length parameters l , all for the same contact radius a and the same strain hardening level, $n = 5$. The plastic zone is estimated as the region in which the effective stress measure is greater than σ_y , or, equivalently, $E_e > 1.3\epsilon_y$, as determined by the stress–strain relationship (8). The size of the plastic zone for the conventional plasticity limit, given approximately for the case $l/a = 0.001$ is consistent with previously published results (e.g. Bhattacharya and Nix, 1991; Giannakopoulos and Larsson, 1997; Shu and Fleck, 1997), regardless of whether flow or deformation plasticity theory was used. Figure 4 illustrates that increasing the material length parameter l , or, equivalently, decreasing the size of the indent a , increases the extent of the plasticity

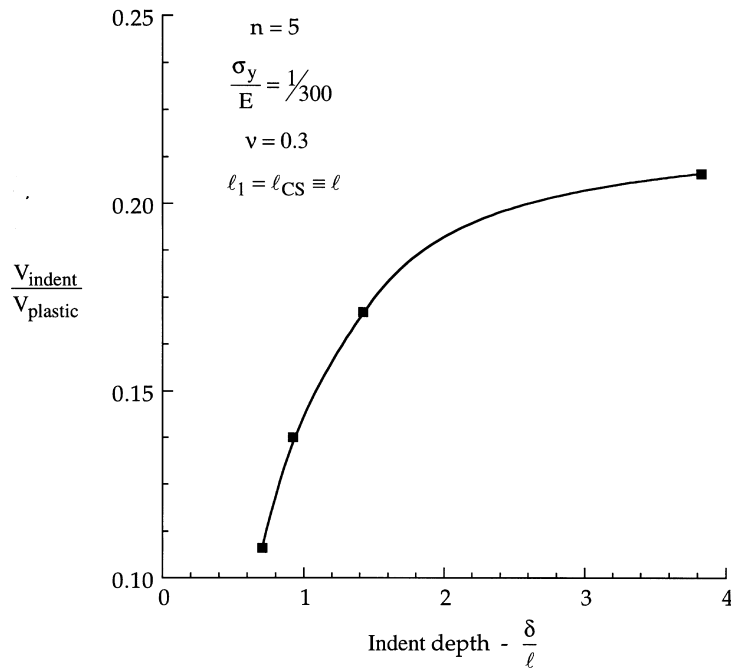


Fig. 5. Ratio of indentation volume over estimated plastic zone volume vs indentation depth. The volume of the plastic zone was estimated by fitting the curves in Fig. 4 with a half-ellipsoid of revolution.

zone relative to the indent size. When the indent radius is as small as $2l$, the extent of the plastic zone is nearly doubled. This is a large effect, but not surprising given the effect of l on the indentation load.

The effect is further illustrated in Fig. 5, which presents the ratio of the indentation volume over the volume of the plastic zone. The volume of the plastic zone was estimated by identifying the plastic zone as the region inside the appropriate contour in Fig. 4 and fitting the shape of the zone with a half-ellipsoid of revolution. Ma and Clarke (1995) have presented experimental results in a similar manner. They estimated the extent of plastic flow by measuring the size of the plastic zone at a given depth. Their results are presented in the same manner as in Fig. 5, with the ratio of indentation volume to plastic zone volume vs indentation depth. Their experiments confirm the trend displayed in Fig. 5: smaller indents have significantly larger relative plastic zone sizes.

4.3. Role of the individual length parameters, l_1 and l_{CS} .

The results presented above are for the SG solid for which the ratio of the amplitudes of the length parameters in (6) are fixed according to $l_1 = l_{CS} \equiv l$ (with $l_2 = \frac{1}{2}l_{CS}$ and

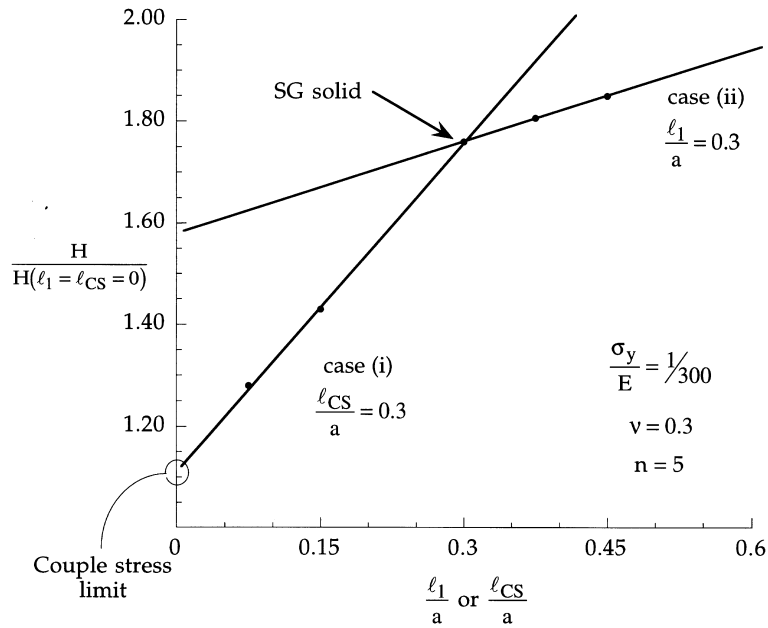


Fig. 6. Normalized hardness predictions as a function of individual length scale parameters; in case (i) l_{CS} is constant and l_1 varies, in case (ii) l_1 is constant and l_{CS} varies.

$l_3 = \sqrt{\frac{5}{24}} l_{CS}$). There is no physical basis for this particular choice of ratio, except that it ensures that both stretch and rotation gradients influence gradient hardening. This choice also ensures that E_e is positive definite because each of the three length parameters, l_i , in (2) are non-zero.

To gain some insight on the role of individual length parameters on hardness, calculations were carried out in which l_1 and l_{CS} were varied independently. Normalized hardness predictions are shown in Fig. 6 for a material with $\sigma_y/E = 1/300$, $n = 5$ and $\nu = 0.3$. Case (i) displays the dependence of the normalized hardness on l_1/a with l_{CS}/a fixed at 0.3, while case (ii) gives the dependence on l_{CS}/a with l_1/a fixed at 0.3. The point where the two curves cross at $l_1/a = l_{CS}/a = 0.3$ is the case of the SG solid. The relative slopes of the two cases illustrate that l_1 has much more effect on the hardness than l_{CS} . A decrease of l_1 by 50% [case (i)] drops the size-dependent hardness elevation by 60%. Conversely, the length parameter associated with the couple stress theory, l_{CS} , plays a relatively insignificant role. A 50% change in l_{CS} only results in approximately a 10% change hardness elevation. The results are consistent with the results of Shu and Fleck (1996), who found the couple stress theory did not predict significant hardness increases. Extrapolating the results for case (i) to $l_1/a = 0$ (see Fig. 6), one finds a size-dependent hardness elevation on the order of 10% for the couple stress solid with $l_{CS}/a = 0.3$. Shu and Fleck report a 5% elevation for this

case; the discrepancy can be explained by minor differences in the assumed tensile stress-strain law (8) and element performance.

An open question remains: What is the relative proportion of the material length parameters l_1 and l_{CS} ? Hopefully, insights will come from fundamental dislocation mechanics. It seems more likely, however, at least in the short term, that the answer will come from correlation with experiments which differentiate the two contributions, such as indentation and wire torsion. The parameter l_{CS} is clearly of secondary importance in indentation. By contrast, as noted earlier, l_1 has no influence on wire torsion. In the present study, a non-zero value of l_{CS} is required to ensure a positive definite formulation for the strain energy density. When the ratio l_{CS}/l_1 is taken to be too small, the finite element model becomes ill-conditioned. Thus, the SG solid with $l_1 = l_{CS} \equiv l$ provides a useful choice in the present study. Identification of l by fitting the solutions for the SG solid to experimental indentation data should be regarded as an approximate determination of l_1 with no implication for l_{CS} .

5. COMPARISON WITH EXPERIMENTS AND DISLOCATION MODELS: CHOICE OF THE MATERIAL LENGTH PARAMETER l

Indentation hardness data of Ma and Clark (1995) on silver single crystals with two orientations relative to the axis of the indenter are shown in Fig. 7(a), and another set of data on tungsten single crystals from Stelmashenko *et al.* (1993) at three orientations are shown in Fig. 7(b). In the first case, the hardness H is plotted against the indentation depth (h), while in the second it is plotted against the indent diagonal (D). Ma and Clarke used a Berkovich indenter (65.3° face angle) with the same area-depth ratio as the Vicker's indenter (68° face angle) used by Stelmashenko *et al.* There is some dependence of the measured hardness on crystal orientation relative to the indentation direction in both sets of data, but size-dependence dominates. Superimposed on the data in Fig. 7 are the present theoretical predictions from Fig. 2 for $n = 3$, corresponding to a high strain hardening level characteristic of annealed metals.

The theoretical predictions were generated in the following manner. The results in Fig. 2 were fitted with second order polynomials to obtain H/H_0 as a function of l/a . The limiting macroscopic hardness ($H_0 \equiv H$ for $l/a = 0$) chosen for the fit is approximately the value of the hardness obtained in the experiments for the largest indent. These values are given in Table 1 and are indicated in each plot in Fig. 7. Indents of the same area are compared; the contact radius in the prediction was related to the experimental depth (or diagonal size) that would give the same projected area. Equating the areas for a 72° cone and a Berkovich indenter yields $a = 2.8h$, where h is the experimental depth. The relationship for a Vickers indenter is $a = 0.45D$, where D is the diagonal of the impression in the experiment.* These equations substituted into the polynomials yields an expression for the predicted hardness as a

* Since the cone used here has a slightly higher area/depth ratio than the Vickers and Berkovich indenters, the depth of the prediction is slightly smaller than the actual depth in the experiments. Using a cone angle of 70.3° gives the same area/depth relation and hence, compares indents of equal area and depth; the equations above would not change.

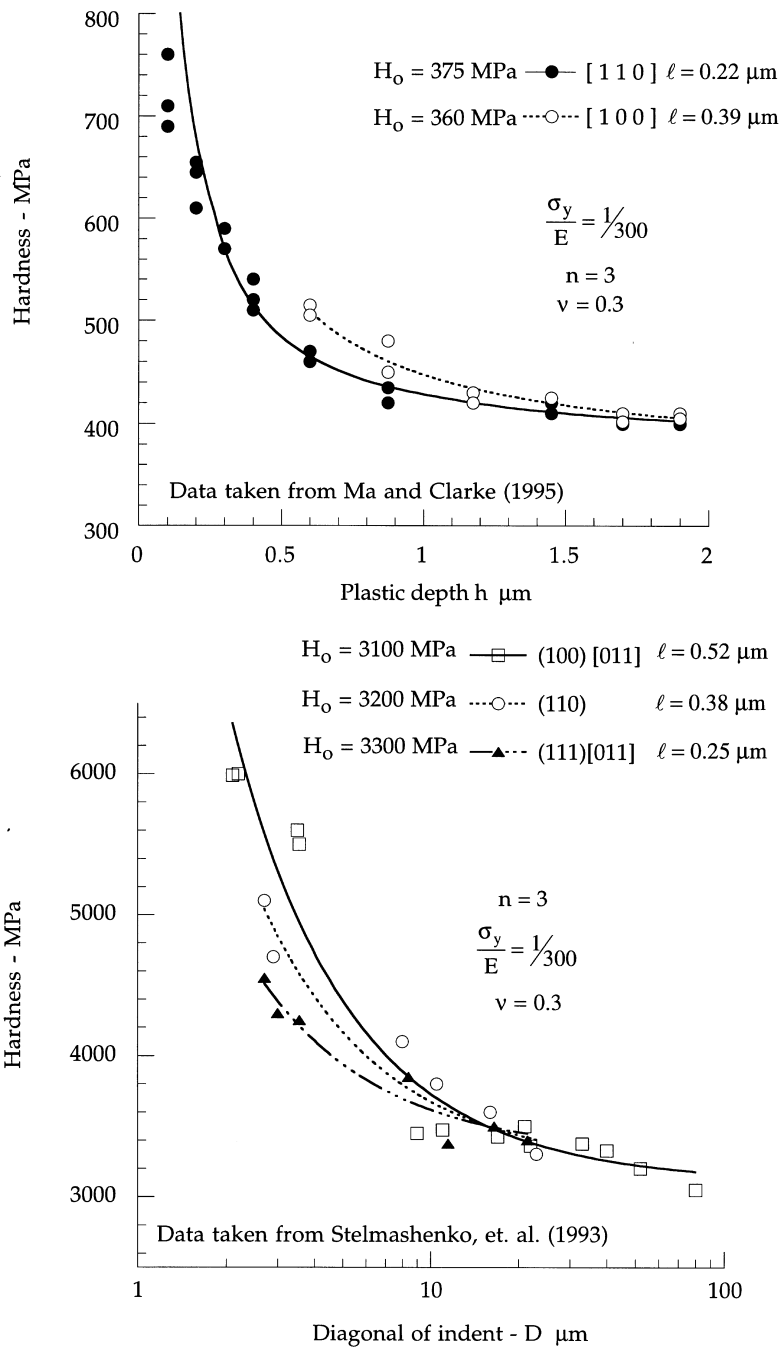


Fig. 7. (a) Comparison of the experimental results of Ma and Clarke (1995) and the theoretical predictions given in Fig. 2. The lines indicate the results of a least squares fit to determine the material length scale. The experiments were done using a Berkovich indenter with a 65.3° face angle. (b) Comparison of the experimental results of Stelmashenko *et al.* (1995) and the theoretical predictions given in Fig. 2. The lines indicate the results of a least squares fit to determine to the material length scale. The experiments were done using a Vickers indenter with a 68° face angle.

function of experimental depth (or diagonal) and the material length scale l . The length scale was then determined by a least squares fit of the functions $H = f(h, l)$ to the experimental data. This was done for both $n = 3$ and $n = 5$, and the results are tabulated in Table 1. For all cases, values for l in the range 0.2–0.6 μm fit the data very well.

For hardnesses which do not exceed the macroscopic hardness, H_0 , by more than a factor of about 2, the numerical results of Fig. 2 can be well approximated by a linear dependence on the inverse indent radius according to

$$\frac{H}{H_0} = 1 + c(n, \sigma_y/E) \frac{l}{a}. \quad (17)$$

For $\sigma_y/E = 1/300$, the numerical results give $c \cong 1.85$ for $n = 3$ and $c \cong 2.43$ for $n = 5$.

A somewhat different dependence of H on the indent size has been suggested on the basis of dislocation arguments by De Guzman *et al.* (1993), Ma and Clarke (1995), Poole *et al.* (1997) and Nix (1997). Here, Nix's (1997) result will be quoted as it is the most detailed. The starting point of each of the above derivations is that the flow stress follows Taylor's relation $\tau = \alpha\mu b\rho^{1/2}$, where α is a constant depending on structure which is about 0.3 for FCC materials, μ is the shear modulus, b is the Burgers vector, and ρ is the total dislocation density. The total dislocation density is taken to be the sum of the statistically stored dislocations, ρ_s , and the geometrically stored dislocations, ρ_G , according to $\rho = \rho_s + \rho_G$. The statistically stored dislocations are related to the average plastic strain, while the geometrically necessary dislocations are tied to the incompatibility of the deformations induced by the indenter. Nix takes $\rho_G = 3(\cot\beta)^2/(16bh)$. His final result for the size-dependent hardness is

$$\left(\frac{H}{H_0}\right)^2 = 1 + \frac{h^*}{h} \quad (18)$$

where $H_0 = 3\sqrt{3}\alpha\mu b\sqrt{\rho_s}$ and $h^* = 3(\cot\beta)^2/(16b\rho_s)$. Note that h^*/h is equivalent to a^*/a , where $a^* = h^*/\cot\beta$. For small values of a^*/a , (18) also gives an inverse dependence on indent size as in (17). The two results are brought into coincidence if

$$c(n, \sigma_y/E)l = \frac{1}{2}a^*. \quad (19)$$

Differences between (17) and (18) become noticeable for values of a^*/a greater than about 1/2.

Nix (1997) plotted data for copper single crystals of McElhaney *et al.* (1997) as $(H/H_0)^2$ vs $1/h$, presented here in Fig. 8. This data is taken with a Berkovich diamond pyramidal indenter with a 65.3° face angle. The linear dependence of $(H/H_0)^2$ with $1/h$ displayed by the data over the range from $h = 1/5$ – $2 \mu\text{m}$ is striking. Nix extrapolated the unnormalized data to $1/h = 0$ to obtain $H_0 = 556 \text{ MPa}$. The value, $h^* = 1.68 \mu\text{m}$, in (18) gives the best fit to the data. Poole *et al.* (1996) also presented plots of H^2 vs $1/h$ for their micro-indentation data on two sets of copper polycrystals, one

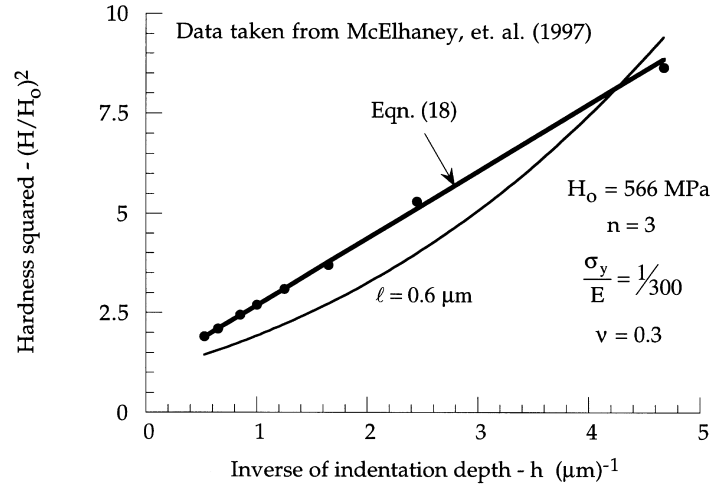


Fig. 8. (a) Comparison of the experimental results of McElhaney *et al.* (1997), the theoretical predictions of Nix [eqn (18)] and the theoretical predictions given in Fig. 2. The experiments were done using a Berkovich indenter with a 65.3° face angle.

annealed and one work hardened. Their data indicates a value of h^* for the work hardened copper, which is roughly one quarter that for the annealed copper. Their data, however, is less convincing as to the linear dependence of $(H/H_0)^2$ on $1/h$.

Superimposed onto Fig. 8 are the numerical results from the present analysis (from Fig. 2) for the case $n = 3$, using $H_0 = 556$ MPa and accounting for the difference between the pyramidal and conical indenters in the manner discussed earlier. The least squares fit outlined earlier results in the value $l = 0.6 \mu\text{m}$. (A summary of the fitting results is included in Table 1.) As mentioned above, the present results do not produce a linear dependence of $(H/H_0)^2$ on $1/h$ over the full range of $1/h$. The dependence of the present results seen in Fig. 8 is a consequence of the composition of the invariants employed in (6). In strain gradient plasticity, strain gradients are associated with geometric dislocations, while statistically stored dislocations are associated with the deviator strains (Fleck and Hutchinson, 1997). Thus, rather than a linear dependence of the form $\rho_S + \rho_G$, the effective strain E_e in (6) models a dependence composed according to the so-called harmonic mean as $\sqrt{\rho_S^2 + \rho_G^2}$. This choice has been made largely for mathematical convenience. Alternative compositions to (6) are discussed by Fleck and Hutchinson which are capable of modeling the linear dependence, $\rho_S + \rho_G$. Specifically, the choice

$$E_e = \left[\left(\frac{2}{3} \varepsilon'_{ij} \varepsilon'_{ij} \right)^{\lambda/2} + \left(l_1^2 \eta_{ijk}^{(1)} \eta_{ijk}^{(1)} + \frac{2}{3} l_{CS}^2 \chi_{ij} \chi_{ij} \right)^{\lambda/2} \right]^{1/\lambda} \quad (20)$$

models the linear dependence for $\lambda = 1$ and reduces to (6) for $\lambda = 2$. Until more data

becomes available, we leave for the future the investigation of whether an alternative composition such as (20) should be used in the strain gradient plasticity formulation.

Finally, the theoretical results in Fig. 2 have been fit to hardness data collected and analyzed by Atkinson (1995). Atkinson conducted indentation tests on a wide range of polycrystalline metals and extensively analyzed the data, with the goal of quantifying the size effect through relatively simple empirical formulae containing parameters to be determined by fitting the experimental hardness trends. One of the significant results of Atkinson's analysis is the finding that the variance of the fitting parameters is not greater for smaller indents than larger indents. This emphasizes that measurement error does not systematically increase with decreasing indent size. Atkinson's took data for relatively large indents, with the radius of the smallest indents no smaller than about $5 \mu\text{m}$. Consequently, his hardness measurements for the smallest indents were no more than 25–35% above the macroscopic hardness values. Atkinson found distinct differences among metals that divided along two lines: metals which were strain hardened by plastic working and those that were annealed. By choosing the material length parameter l for the present results in Fig. 2 to fit Atkinson's data for a given class of metals, we were able to accurately reproduce the variation of H/H_0 with indent size. Typically, the value of l for an annealed (soft) metal was found to be about $1.6 \mu\text{m}$. The corresponding value for a work hardened (hard) metal was between $1/2$ and $1 \mu\text{m}$. The values given in Table 1 are the results to fitting average results presented in Atkinson's paper.

In summary, indentation data appears to be an excellent means to infer the material length scale l in the strain gradient plasticity theory. As emphasized in Section 4, l should be identified with the length parameter l_1 associated with stretch gradients in (6), since l_{CS} has little influence on indentation. The values of l inferred from experimental data for a number of materials lies with the range for about $1/4$ – $1 \mu\text{m}$, with the hardest materials having the smallest values of l . This is consistent with the fact that the free slip distance of dislocations decreases with hardness, and that l is related to the free slip distance.

ACKNOWLEDGMENTS

This work was supported in part by the ONR through Grant N00014-96-10059, by the NSF through Grant NSF-CMS-96-34632, and by the Division of Engineering and Applied Sciences, Harvard University.

REFERENCES

- Acharya, A. and Bassani, J. L. (1996) On non-local flow theories that preserve the classical structure of incremental boundary value problems. In *IUTAM Symposium on Micromechanics of Plasticity and Damage*, ed. A. Pineau and A. Zaoui, pp. 3–10. Kluwer Academic Publishers.
- Acharya, A. and Bassani, J. L. (1997) Incompatibility and crystal plasticity. To be published.
- Atkinson, M. (1995) Further analysis of the size effective in indentation hardness tests of some metals. *J. Mater. Res.* **10**, 2908–2915.

- Atkins, A. G. and Tabor, D. (1965) Plastic indentation in metals with cones. *Journal of the Mechanics and Physics of Solids* **13**, 149–164.
- Bhattacharya, A. K. and Nix, W. D. (1991) Finite element analysis of cone indentation. *International Journal of Solids and Structures* **27**, 1047–1058.
- Brown, L. M. (1997) Transition from laminar to irrotational motion in plasticity. To be published.
- De Guzman, M. S., Neubauer, G., Flinn, P. and Nix, W. D. (1993) The role of indentation depth on the measured hardness of materials. *Mater. Res. Symp. Proc.* **308**, 613–618.
- Doerner, M. F. and Nix, W. D. (1986) A method for interpreting the data from depth sensing indentation measurements. *J. Mater. Res.* **1**, 601–609.
- Fleck, N. A. and Hutchinson, J. W. (1993) A phenomenological theory for strain gradient effects in plasticity. *Journal of the Mechanics and Physics of Solids* **41**, 1825–1857.
- Fleck, N. A. and Hutchinson, J. W. (1997) Strain gradient plasticity. In *Advances in Applied Mechanics*, ed. J. W. Hutchinson and T. Y. Wu, Vol. 33. Academic Press, New York.
- Fleck, N. A., Muller, G. M., Ashby, M. F. and Hutchinson, J. W. (1994) Strain gradient plasticity: theory and experiment. *Acta Metallica Materiala* **42**, 475–487.
- Gane, N. and Cox, J. M. (1970) The microhardness of metals at very low loads. *Philos. Mag.* **22**, 881–891.
- Giannakopoulos, A. E. and Larsson, P.-L. (1997) Analysis of pyramid indentation of pressure-sensitive hard metals and ceramics. *Mech. Matls* **25**, 1–35.
- Johnson, K. L. (1970) The correlation of indentation experiments. *Journal of the Mechanics and Physics of Solids* **18**, 115–126.
- Ma, Q. and Clarke, D. R. (1995) Size dependent hardness of silver single crystals. *J. Mater. Res.* **10**, 853–863.
- McElhane, K. W., Vlassak, J. J. and Nix, W. D. (1997) *J. Mater. Res.*, to be published.
- Mindlin, R. D. (1965) Micro-structure in linear elasticity. *Arch. Ration. Mech. Anal.* **16**, 51–78.
- Nix, W. D. (1997) Elastic and plastic properties of thin films on substrates: nanoindentation techniques. *Mat. Sci. and Engr. A*, **234–236**, 37–44.
- Pethica, J. B., Hutchings, R. and Oliver, W. C. (1983) Hardness measurements at penetration depths as small as 20 nm. *Philos. Mag.* **A48**, 593–606.
- Poole, W. J., Ashby, M. F. and Fleck, N. A. (1996) Micro-hardness tests on annealed and work-hardened copper polycrystals. *Scripta Metall. Mater.* **34**, 559–564.
- Rubenstein, C. (1981) A critical appraisal of static hardness measurements. *Journal of Applied Mechanics* **48**, 796.
- Samuels, L. E. (1986) *Microindentation Techniques in Materials Science and Engineering*, ed. P. J. Blau and B. R. Law, pp. 5–24. ASTM STP 880, American Society for Testing and Materials, Philadelphia, PA.
- Shu, J. and Fleck, N. A. (1997) The prediction of a size effect in micro-indentation. *International Journal of Solids and Structures*, submitted.
- Shu, J. Y., King, W. E. and Fleck, N. A. (1997) Finite elements for materials with strain gradient effects. *International Journal of Numerical Methods in Engineering*, submitted.
- Smyshlaev, V. P. and Fleck, N. A. (1996) The role of strain gradients in the grain size effect for polycrystals. *Journal of the Mechanics and Physics of Solids* **44**, 465–496.
- Specht, B. (1988) Modified shape functions for the three node plate bending element passing the patch test. *International Journal of Numerical Methods in Engineering* **26**, 705–715.
- Stelmashenko, N. A., Walls, M. G., Brown, L. M. and Miman, Y. V. (1993) Microindentation on W and Mo oriented single crystals: An SEM study. *Acta Metallica Materiala* **41**, 2855–2865.
- Toupin, R. A. (1962) Elastic materials with couple stresses. *Arch. Ration. Mech. Anal.* **11**, 385–414.
- Xia, Z. C. and Hutchinson, J. W. (1996) Crack tip fields in strain gradient plasticity. *Journal of the Mechanics and Physics of Solids* **44**, 1621–1648.
- Zienkiewicz, O. C. and Taylor, R. L. (1989) *The Finite Element Method: Volumes I and II*, 4th edn. McGraw-Hill, London.

APPENDIX

Table A1. *Non-zero strain gradients for the general axisymmetric case*

Deviatoric strain gradients	Non-deviatoric components	Derivative components
η'_{rrr}	$\frac{1}{2}\eta_{rrr} - \frac{1}{2}(\eta_{r\theta\theta} + \eta_{rzz})$	$\frac{1}{2}\frac{\partial^2 u_r}{\partial r^2} - \frac{1}{2}\left(\frac{1}{r}\frac{\partial u_r}{\partial r} - \frac{u_r}{r^2} + \frac{\partial^2 u_z}{\partial r \partial z}\right)$
η'_{rrz}	η_{rrz}	$\frac{\partial^2 u_z}{\partial r^2}$
$\eta'_{r\theta\theta} = \eta'_{\theta r\theta}$	$\frac{3}{4}\eta_{r\theta\theta} - \frac{1}{4}(\eta_{rrr} + \eta_{rzz})$	$\frac{3}{4}\left(\frac{1}{r}\frac{\partial u_r}{\partial r} - \frac{u_r}{r^2}\right) - \frac{1}{4}\left(\frac{\partial^2 u_r}{\partial r^2} + \frac{\partial^2 u_z}{\partial r \partial z}\right)$
$\eta'_{rzz} = \eta'_{zrr}$	$\frac{3}{4}\eta_{rzz} - \frac{1}{4}(\eta_{r\theta\theta} + \eta_{zzz})$	$\frac{3}{4}\frac{\partial^2 u_r}{\partial r \partial z} - \frac{1}{4}\left(\frac{1}{r}\frac{\partial u_z}{\partial z} + \frac{\partial^2 u_z}{\partial z^2}\right)$
$\eta'_{rzz} = \eta'_{zrz}$	$\frac{3}{4}\eta_{rzz} - \frac{1}{4}(\eta_{rrr} + \eta_{r\theta\theta})$	$\frac{3}{4}\frac{\partial^2 u_r}{\partial r \partial z} - \frac{1}{4}\left(\frac{\partial^2 u_r}{\partial r^2} + \frac{1}{r}\frac{\partial u_r}{\partial r} - \frac{u_r}{r^2}\right)$
$\eta'_{\theta\theta r}$	$\eta_{\theta\theta r}$	$\frac{1}{r}\frac{\partial u_r}{\partial r} - \frac{u_r}{r^2}$
$\eta'_{\theta\theta z}$	$\eta_{\theta\theta z}$	$\frac{1}{r}\frac{\partial u_z}{\partial r}$
$\eta'_{\theta z\theta} = \eta'_{z\theta\theta}$	$\frac{3}{4}\eta_{\theta z\theta} - \frac{1}{4}(\eta_{zrr} + \eta_{zzz})$	$\frac{3}{4}\frac{1}{r}\frac{\partial u_r}{\partial z} - \frac{1}{4}\left(\frac{\partial^2 u_r}{\partial r \partial z} + \frac{\partial^2 u_z}{\partial z^2}\right)$
η'_{zzz}	$\frac{1}{2}\eta_{zzz} - \frac{1}{2}(\eta_{zrr} + \eta_{z\theta\theta})$	$\frac{1}{2}\frac{\partial^2 u_z}{\partial z^2} - \frac{1}{2}\left(\frac{\partial^2 u_r}{\partial r \partial z} + \frac{1}{r}\frac{\partial u_z}{\partial r}\right)$
η'_{zzr}	η_{zzr}	$\frac{\partial^2 u_r}{\partial z^2}$

Table A2. *Hardness predicted for conventional plasticity*

	$(\sigma_y/E) = 1/300$; $\nu = 0.3$; $(l/a) = 0.001$ $(\bar{H}/\sigma_y) = (P/\sigma_y \pi a^2)$	Approximate δ/a
$n = 3$	7.49	0.37
$n = 5$	5.57	0.35
$n = 10$	3.85	0.33